Title

Novel Numerical Method for Parameterising Fretting Contacts

Authors

A. Wade[a], R. Copley[b], A. Alsheikh Omar[a], B. Clarke[b], T. Liskiewicz[a] and M. Bryant[a]

[a] *University of Leeds, School of Mechanical Engineering, Institute of Functional Surfaces, Leeds, UK;*

[b] *University of Sheffield, School of Mechanical Engineering, Leonardo Tribology Centre, Sheffield, UK.*

Abstract

Fretting regime transition is traditionally achieved by qualitative assessment of the fretting loops (tangential force , Q vs tangential displacement δ) and material response. Other studies used parameters in which thresholds are theoretically determined to exceed friction at the contact for regime transition identification. This study successfully developed a flexible loop analysis method based on simple vector principles that is able to quantify and characterise its constituent parts. In terms of fretting contact analysis the loop analysis method provided a complementary method of regime transition identification to those based on theoretically overcoming friction at the contact, with strong agreement between the two. This novel method provides an efficient way to correlate regime transition with other data sets, with additional insights into the mechanical response of the contact compared to other regime transition criteria. Possible applications of this method include enabling smart asset monitoring and in the development of engineering components that are subject to fretting. This is an extremely flexible technique that has applicability for other types of loop analysis.

Keywords/Phrases

Fretting, regime, transition, loop analysis and, numerical method.

1. Introduction

Fretting is relatively small-amplitude oscillatory movement between two surfaces. The small-amplitude nature means that detection is difficult, resulting in either catastrophic failure or expensive maintenance programmes [1,2]. It occurs in many systems that are subject to cyclic loads such as: suspension cables, dovetail joints in turbine engines, electrical contacts and heat exchangers [3]. There is an intimate link with corrosion leading to a complex degradation mechanism [4]. Orthopaedic implants are one such example where fretting-corrosion is a significant degradation mechanism leading to early failure [5,6]. Depending on the working conditions, different regimes can be achieved and are associated with different degradation mechanisms [7]. The partial slip regime (PSR) is more commonly associated with fretting fatigue crack formation and the gross slip regime (GSR) with fretting wear. The regime acting at an interface is dependent on a number of different variables. However, within a given contact this is predominately determined by normal load (W) and tangential force (Q) or displacement (δ) [8]. Running condition fretting maps (W vs δ) of particular contacts are a convenient way to demonstrate how transition is achieved [9]. Transition from PSR to GSR can be achieved by either increasing δ above a critical amount to overcome the dominant

elastic deformation of the contact under a constant normal load or, decreasing W below a critical amount with a constant δ.

Considering a Hertzian contact, different regimes demonstrate characteristic fretting loops (Q vs δ graphs) and material responses [7,8]. PSR fretting loops demonstrate a narrow hysteresis loop associated with plastic shear and fatigue crack formation. Mindlin was the first to introduce the presence a central stick region with limited degradation due to sufficient normal stress to prevent slip, surrounded by an outer slip region where normal stress is insufficient in preventing slip [10]. The GSR fretting loop displays a larger elongated hysteresis loop. This larger loop is associated with surface and bulk plastic deformation and shearing of connecting asperities for fretting wear. The mixed fretting regime (MFR) is where transition between the GSR and PSR exists under constant working conditions close to critical values of δ and W, resulting in highly transient and unpredictable processes at the interface [11]. Fretting contacts are extremely complex and transient in nature due to the cyclic loading where material can either escape or be retained altering the working conditions with time [12,13]. Further complication and interactions can arise from humidity, oxide formation and presence of boundary lubricants [4,14]. The tribologically transformed structure is one such reported phenomena which illustrates how these factors can interact [15].

Traditionally, qualitative assessment of the shape of the fretting loops and material response were used to differentiate between regimes [7,8]. Other studies have attempted to assess transition in a more objective manner using Mindlin's slip ratio [16], progression of the coefficient of friction (μ) [17,18], fretting energy dissipation (ratio, A)[18–21], slip ratio (D) [18,20,22–24] and slip index (δ_i)[25]. Table 1 details the transition criteria used by literature.

Table 1 Summary of used transition criteria by literature.

Parameter	Expression	Threshold Value(s)/ Transition Criteria
Mindlin's Slip Ratio [10]	$\frac{a'}{a} = \left(1 - \frac{Q}{\mu W}\right)^{\frac{1}{3}}$	$0 < \frac{a'}{a} < 1$ PSR $\frac{a'}{a} = 1$ GSR
Coefficient of Friction [18]	$\mu = \frac{Q}{W}$	When the static coefficient of friction has been overcome and no longer varies with tangential displacement amplitude (δ).
Energy Ratio [18]	$A = \frac{E_d}{E_t} = \frac{Dissipated\ Energy}{Total\ Energy}$	$A \leq 0.2$ PSR $A > 0.2$ GSR
Slip Ratio [18]	$D = \frac{\delta_0}{\delta^*} = \frac{Displacement\ Amplitude\ at\ zero\ Q}{Maximum\ Displacement\ Amplitude}$	$D \leq 0.26$ PSR $D > 0.26$ GSR
Slip Index [25]	$\delta_i = \frac{\delta^* S_c}{W} = \frac{Displacement\ Amplitude \times Elastic\ Slope\ of\ friction\ Loop}{Normal\ load}$	$0.5 \leq \delta_i < 0.6$ PSR $0.8 < \delta_i < 10$ GSR

The ability to use parameters to differentiate between regimes has allowed correlation to other data sets, enabling the innovation of asset monitoring devices. Ito et al. found that peaks in acoustic emission did not occur in the PSR but occurred in the GSR when pure slip was achieved i.e. increase in tangential displacement without an increase tangential force [17]. Mindlin's ratio is a purely theoretical value and based on assumptions which are difficult to qualify. The progression of friction coefficient (CoF) used to identify regime transition requires observation throughout experiments or using predetermined values of $'\mu'$ [18]. Dissipated fretting energy (area bound by the fretting loop, E_d) has found to experience a sudden dramatic increase or decrease during regime transition [19]. Fretting energy and total energy (area bound by the smallest possible rectangle containing a fretting loop, E_t) ratio (A) threshold allows instantaneous identification of regime by theoretically determining when static friction has been overcome [18,20,21,26]. This method provides an approximation of fretting loop shape variation and transition identification, however provides limited insight into the amount of material compliance and an understanding of what is happening at the contact [18,20]. The sliding amplitude to displacement amplitude ratio (D) is an alternative method of identifying regime transition[22,24]. Where a ratio 0.3 and below was the PSR and above 0.4 the GSR, based on theoretically overcoming static friction at a ratio of 0.26 [11,18]. However, measuring and differentiating between slip amplitude and displacement amplitude in practice can be difficult and introduces a certain level of error. The Buckingham-π theorem was used to define slip ratio as a

function of contact stiffness (S_c), displacement amplitude (δ^*) and normal load (W) otherwise known as slip index (δ_i) [25]. Regime transition using the slip index was established by experimentally observing the relationship with the CoF, providing a transition criteria independent of the system and fretting rig mechanical response. However, the transition points between PSR and GSR using this method differed from transition points identified by the slip ratio. Suciu and Uchida developed a fretting loop simulation where ellipse, super ellipse and parallelogram can model the fretting loops for different regimes [24]. They hypothesised that "ellipticity" and rotation of the ellipse can allow regime identification. Heredia and Fouvry, used the percentage number of gross slip cycles in an experiment to aid the identification of critial working conditions, more specifically critical values of δ, by objectively identifying between the GSR, MFR and PSR [23].

The ability to quantify and characterise the mechanical response of a fretting contact to determine between fretting regimes, in an objective and empirical method, can provide a repeatable and robust detection method. This paper details the development of a numerical method that provides accurate, precise and objective fretting regime identification and quantification in real time. This numerical method was based on experimental fretting data but has applicability for other types of loop analysis.

2. Materials and Methods

2.1. Experimental set up

A bespoke in-house built fretting tribometer was used in this study, a 3D Schematic of which can be seen in Fig. 1. The tribometer consisted of an electrodynamic shaker (GWV55/PA300E, Signal Force) which produced oscillatory tangential displacements and a cantilever system which applied normal load (W) through the contact. Tangential load (Q) was measured using a load cell in the shaker arm and tangential displacement was measured using an optical displacement sensor which reflected from an attachment on the shaker arm. Fretting rig control and mechanical data acquisition were achieved using a LabVIEW programme. The contact geometry was a bearing steel ball, diameter $12.7\ mm$ (E_{ball} = 180 GPa, v_{ball} = 0.3) on a flat X65 carbon steel disk (E_{flat} = 200 GPa, v_{flat} = 0.3).

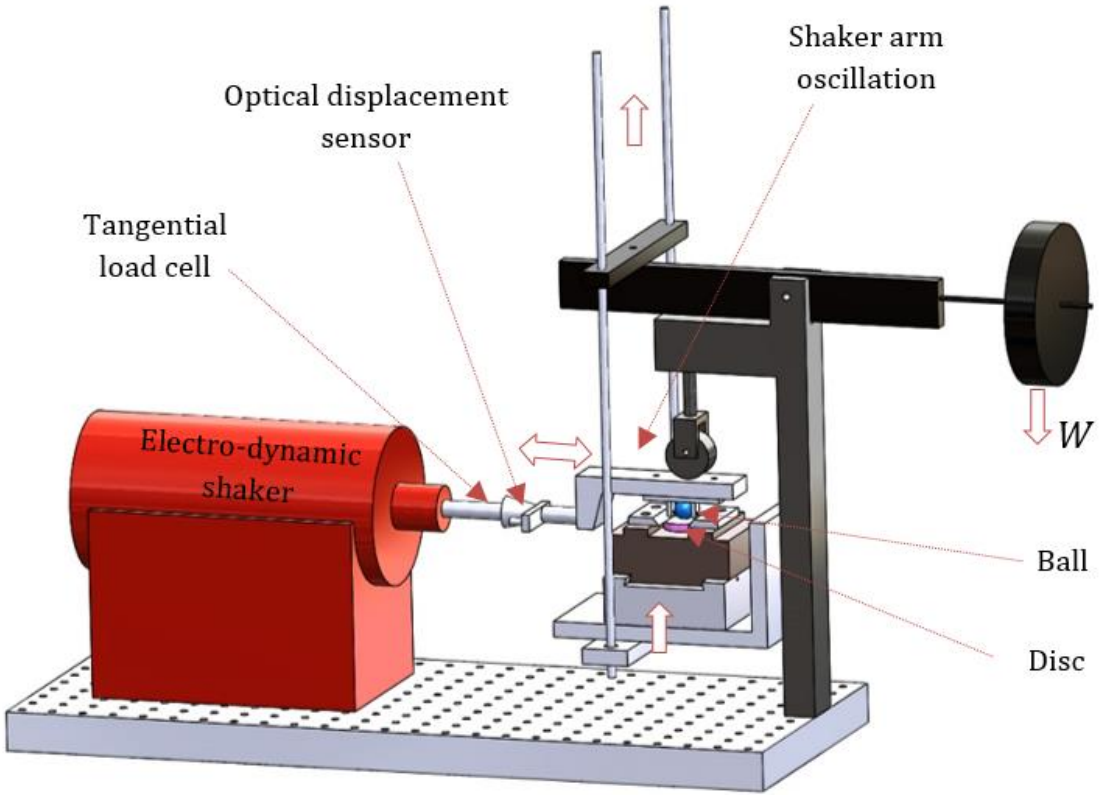

Fig. 1 3D Schematic of experimental set up.

The fretting experiments all ran at a frequency of 3 Hz, with normal load of 50 *N* providing a Hertzian mean contact pressure of approximately 917 MPa. The experiments ran for $1{,}500$ cycles which allowed the fretting rig to achieve a steady state after a period of running-in. The length of this running-in period varied between the different experiments, decreasing with increasing tangential displacement (δ^*), for example at $\delta^* = \pm 100\ \mu m$ the running period ended at around 350 cycles while the running-in period ended at around 1050 cycles at $\delta^* = \pm 25\ \mu m$ as shown in Fig. 5 and Fig. 8. Three repeats were undertaken at each tangential displacement amplitude (δ^*): 25, 50, 75 and 100 μm. Tangential force (Q) and tangential displacement (δ) from the fretting rig were recorded at *600 Hz* and exported to allow analysis using Matlab (R2017b, MathWorks).

2.2. Numerical Analysis

Characterisation of the fretting loops was performed by identifying the proportions due to elastic material response and pure slip (see Fig. 2). This was done by calculating the vector direction and magnitude between two consecutive data points within a fretting loop and repeated for all data points (Fig. 2a and b). The calculated vectors were then sorted and binned into $'N'$ equally spaced direction categories, the range of each direction category equal to that of $180°$ divided by N. This study considered the each vector as a line of travel and as such binned vectors of opposing direction into the same category, as shown in Fig. 2c.

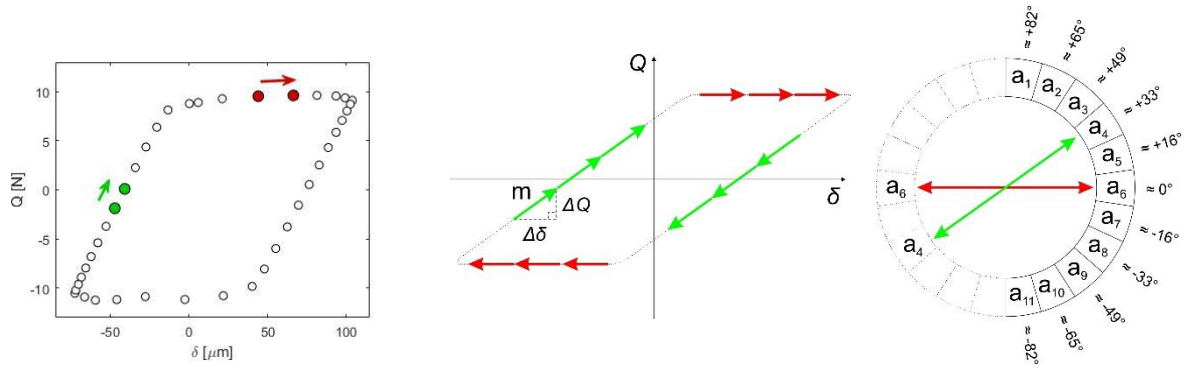

(a) (b) (c)

Fig. 2 Schematics showing progression of numerical analysis method (a) example plot of raw data Q against δ with fewer data points for visual representation, (b) illustration of vector magnitude (m) and vector direction calculation between each point in a fretting loop and (c) schematic of the 11 categories created to characterise the fretting loops without convolution. NB the approximate angles the categories (where $N = 11$) correspond to approximately $\pm 8.2°$ to that stated in this figure.

This experiment used a value of $N = 11$, providing adequate detail for characterisation without convolution. Fig. 3 shows the effects of changing 'N' for this study's particular contact stiffness. Smaller values of 'N' increase the range of angles for each category, and risk losing information where vectors indicating different responses can become grouped together causing inconclusive results (e.g. when $N = 5$ both 0° and 16° fall within the same category as shown in Fig. 3). Increasing 'N' distributes data between neighbouring categories reducing the overall significance of any one category (e.g. where $N = 121$ Fig. 3, the elastic response of the fretting loop was split into three categories). Although a higher resolution can be achieved with a greater value of N, for the purposes of regime transition identification $N = 11$ was adequate as indicated by Fig. 3. An odd number for 'N' was also used to provide a convenient category for pure slip i.e. no increase in Q with increasing δ. The other categories provided easy identification of when friction at the contact was exceeded and provided information on the contact compliance. However, the category system can be changed to suit individual system setups.

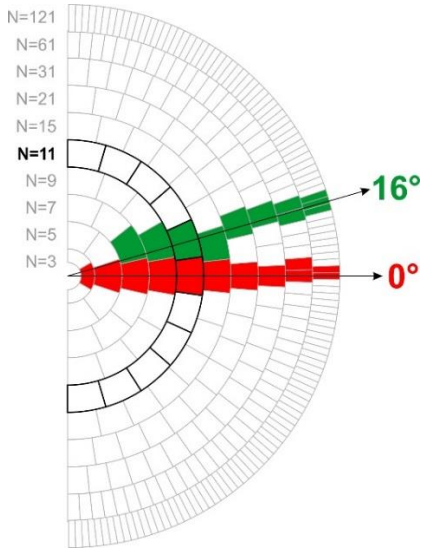

Fig. 3 Schematic demonstration of the effect of increasing or decreasing 'N' for this study's particular contact stiffness.

The vector direction category (a) and magnitude (m) were calculated using simple trigonometry (Eq. 1) and Pythagoras' theorem (Eq. 2).

$$a_n = \left\lceil N\left(\frac{90 - \tan^{-1}(\Delta Q/\Delta\delta)}{180}\right)\right\rceil \quad (1)$$

$$m = \sqrt{\Delta\delta^{\,2} + \Delta Q^2} \quad (2)$$

Where $\Delta\delta$ is the change in tangiential displacement between the two data points and ΔQ is the change in tangiential force between the two data points. This allowed proportional composition of the fretting loops to be calculated and investigated as the experiments progressed. This was achieved by plotting the the catagories and the sum of all the catagories (i.e. the summed vector magnitude of a whole loop) on the same axis to demonstrate shape and size progression. Clearer visulisation of proportional fretting loop composition was achieved by plotting normalised proportional compositions.

This study employed an element of data smoothing by collecting fretting loops into groups of ten before the proportional compositions were determined. Fig. 4 shows the difference in vector analysis on a loop by loop basis and by grouping the loops into ten before proportional composition determination. This provided clear fretting loop characterisation as demonstrated in Fig. 4, which plots percentage a_6, corresponding to gross slip.

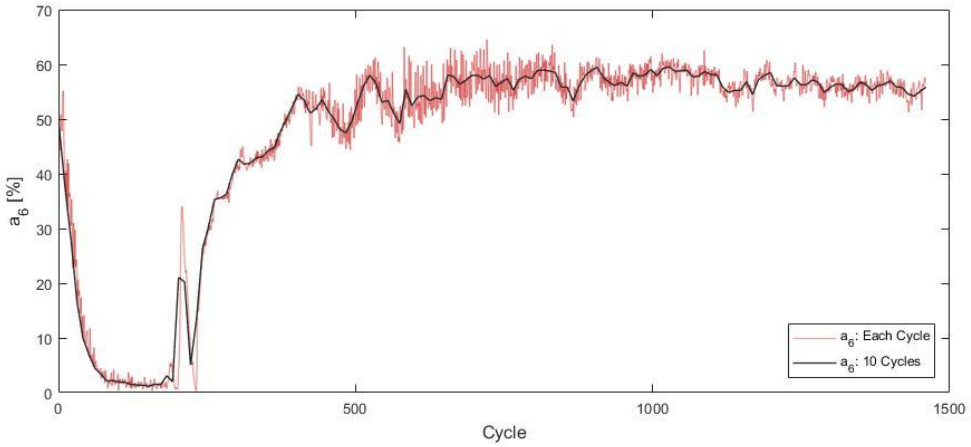

Fig. 4 Example plot of the percentage a_6 over ten cycles compared to every cycle.

Fretting energy (E_d) was calculated as area bound by the fretting loop using the "polyarea" Matlab function. Total dissipated energy (E_t) was approximated as the area of the smallest rectangle able to contain each fretting loop.

3. Results

At δ^* = ± 25 μm the contact was in the PSR, demonstrated by the narrow hysteresis loops (Fig. 5a) and absence of the approximately horizontal relationship between Q and δ. Fretting energy ratio (E_d/E_t) showed a gradual but, negligible increase as the experiment progressed, never exceeding the threshold of 0.2 indicating that static friction had not been exceeded [18] (Fig. 5b). The fretting loops were predominately composed of a_5 (the $+16°$ category) which correlated to the contact stiffness. Other categories were negligible and were therefore not plotted a_6 (the $0°$ category) was

also negligible consistent with the static friction of the interface not being exceeded, see Fig. 5c and d. Considering thresholds for fretting energy ratio and slip ratio that indicate the onset of the GSR [18]; this study utilised a $10\ \%$ fretting loop composition of a_6 threshold. Where if more than $10\ \%$ of the fretting loop was composed of pure slip (a_6) it was considered to be firmly within the GSR, independent of the contact geometry. The normalised fretting loop proportional composition plots clearly show that the percentage composition of a_6 was firmly below the 10 % threshold throughout the experiment indicating the PSR.

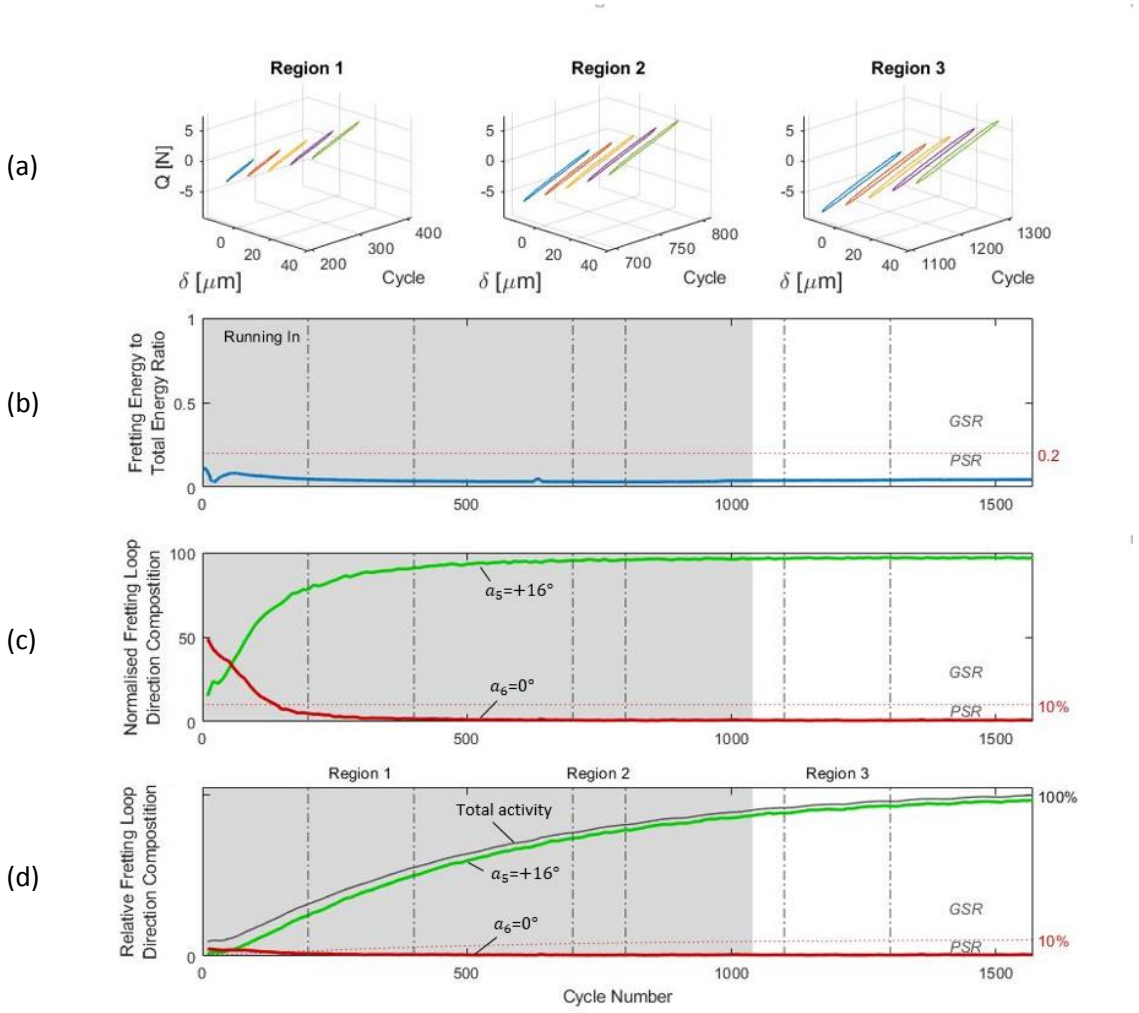

Fig. 5 The $\delta^* = \pm 25\ \mu m$ experiment, (a) fretting loops from three regions demonstrating representative fretting behaviour throughout the experiment: (i) Region 1 at the start (ii)Region 2 mid test and (iii) Region 3 towards the end, (b) fretting energy to total energy ratio with the 0.2 threshold indicated, (c) normalised percentage fretting loop direction composition with 10 % threshold and, (d) the relative fretting loop direction composition with indicated 'Total activity' indicating 100 % total fretting loop vector magnitude (i.e. the total perimeter of the fretting loop) and threshold at 10% of the total activity. The running in period is indicated as the shaded grey region in b, c and d.

At δ^* = ± $50\ \mu m$ experiment contact was within the MFR. This was demonstrated by narrow hysteresis loops, which transitioned after the running-in period, over region *2* in Fig. 6a. Fretting energy ratio (Fig. 6b) presented an increase from around 0.05 to around 0.33. There was a strong correlation between the fretting energy ratio and changes in a_6, comparing Fig. 6b and d.

Importantly, the transition over the threshold of 0.2 was seen at a similar number of cycles as when the 10 % threshold was crossed by the a_6 proportional composition (cycle number 620 and 610 when comparing Fig. 6b to c). The fretting loops were predominately composed of a_5 prior to transition (Fig. 6c and d). After transition, a_6 became more prominent, varying between 30 and 40 % of the total vector magnitude. Interestingly, the magnitude of a_5 remained constant as shown in Fig. 6d corresponding to friction at the contact being overcome, while changes in total magnitude were a function of changes in a_6.

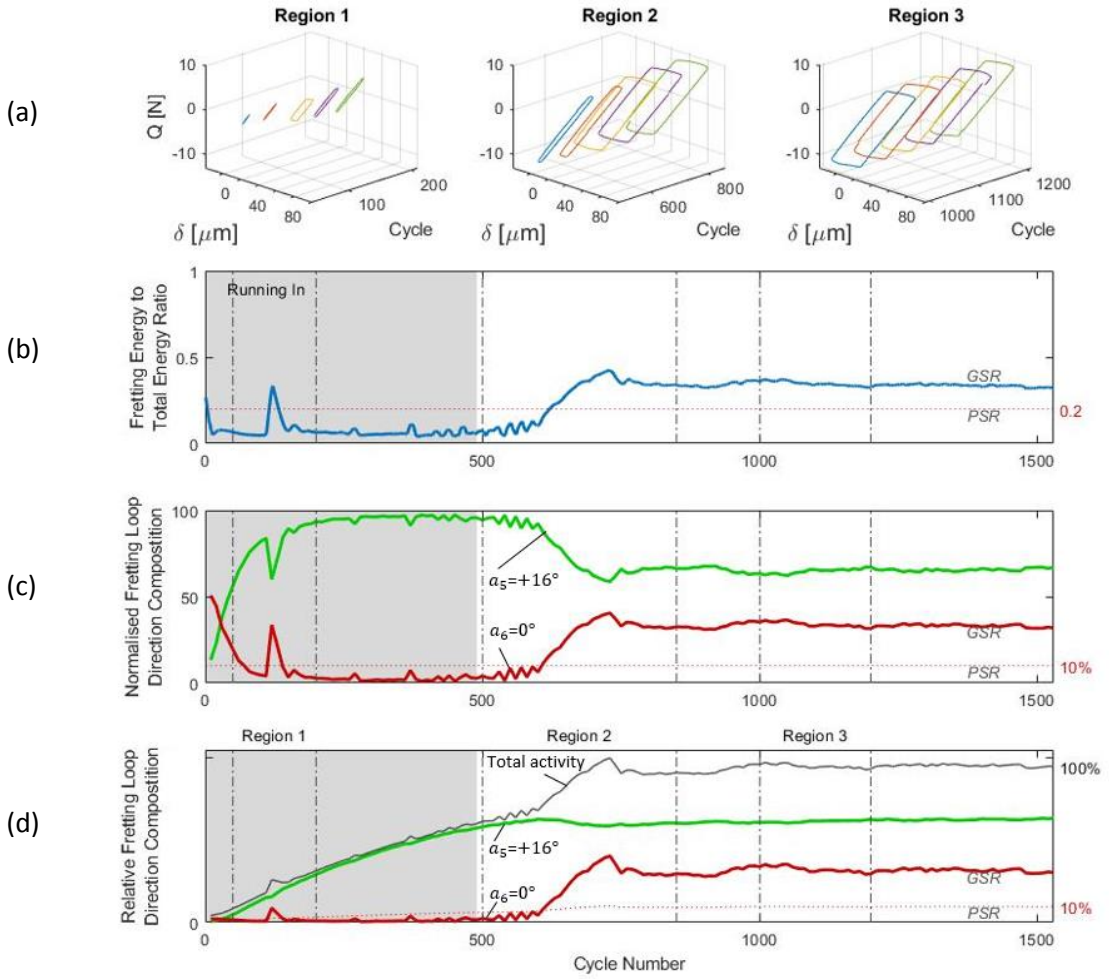

Fig. 6 The δ^* $\pm$50 μm experiment, *(a) fretting loops from three regions demonstrating representative fretting behaviour throughout the experiment: (i) Region 1 within the running-in period (ii) Region 2 over transition according to the* 10 % a_6 *and 0.2 energy ratio thresholds and (iii) Region 3 once the experiment had fully developed, (b) fretting energy to total energy ratio with the 0.2 threshold indicated, (b) fretting energy to total energy ratio with the 0.2 threshold indicated, (c) normalised percentage fretting loop direction composition with 10 % threshold and, (d)* the relative fretting loop direction composition with indicated 'Total activity' indicating 100 % total fretting loop vector magnitude (i.e. the total perimeter of the fretting loop) *and threshold at 10% of the total activity. The running in period is indicated as the shaded grey region in b, c and d.*

The δ^* = ±75 μm experiment was in the GSR demonstrated by the plots of representative fretting loops (Fig. 7a). Transition occurred over Region 1 in Fig. 7a within the running-in period (Fig. 7c, d). The fretting loops demonstrated larger proportion of horizontal relationship than the δ^* = ± 50 μm experiment. Fretting energy ratio presented a significant increase from around 0.15 to around 0.5.

Again, there was a strong correlation between fretting energy ratio and changes in a_6 composition (comparing Fig. 7b and d). The threshold of 0.2 for the fretting energy ratio was crossed at a very similar cycle number as the 10% a_6 threshold. Again, the magnitude of a_5 remained constant after transition (Fig. 7d), and changes in total magnitude are a function of a_6 activity corresponding to friction at the contact being overcome.

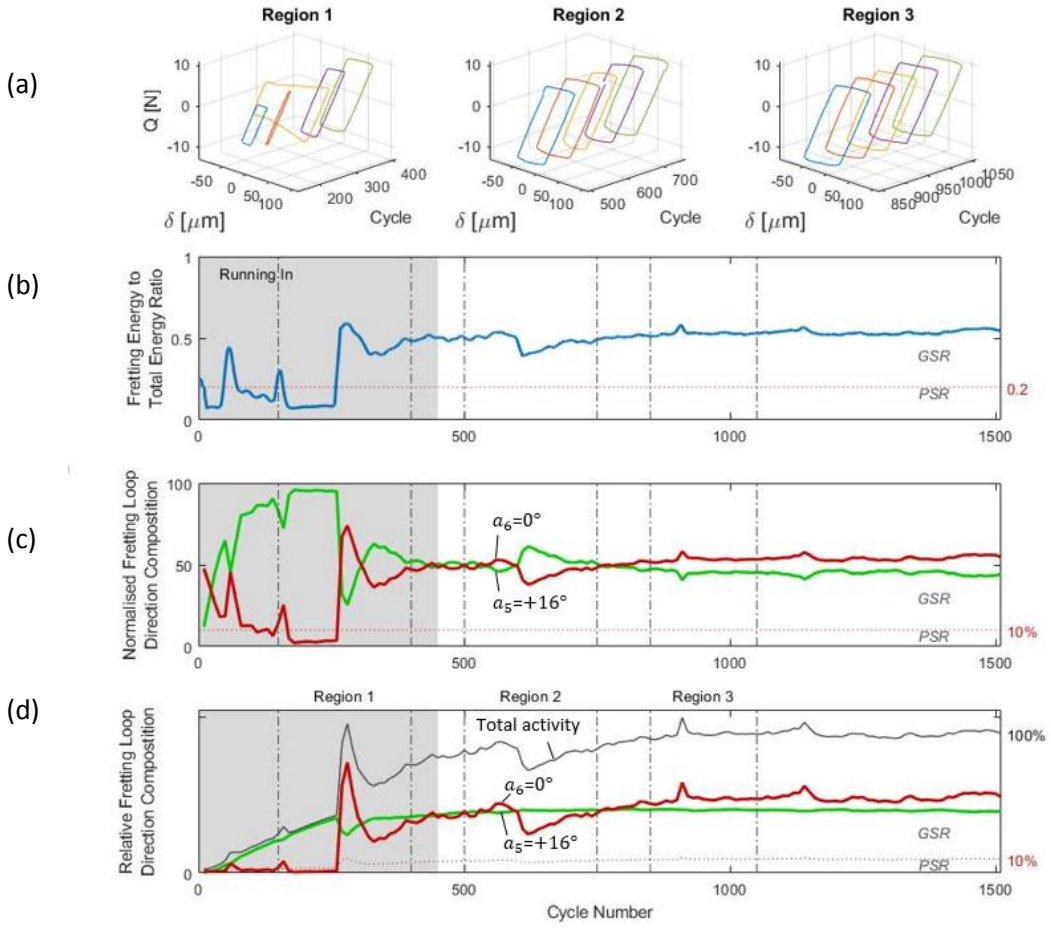

Fig. 7 The δ^* = ±75 μm experiment, *(a) fretting loops from three regions demonstrating representative fretting behaviour throughout the experiment: (i) Region 1 over transition according to the* 10 % a_6 *and 0.2 energy ratio thresholds (ii) Region 2 mid test and (iii) Region 3 towards the end of the test, (b) fretting energy to total energy ratio with the 0.2 threshold indicated, (b) fretting energy to total energy ratio with the 0.2 threshold indicated, (c) normalised percentage fretting loop direction composition with 10 % threshold and, (d)* the relative fretting loop direction composition with indicated 'Total activity' indicating 100 % total fretting loop vector magnitude (i.e. the total perimeter of the fretting loop) and threshold at 10% of the total activity. *The running in period is indicated as the shaded grey region in b, c and d.*

The δ^* = ±100 μm experiment was in the GSR after the transition within the running-in period over Region 1 in Fig. 8a. The hysteresis loops displayed a large proportion of horizontal relationship, greater than the δ^* = ±75 μm experiment. There was a strong correlation between the fretting energy ratio and changes in a_6 comparing Fig. 8 b and d. Again, transition suggested by the 0.2 threshold for fretting energy ratio occurred at a very similar point at the transition point suggested by the a_6 10% threshold. After running-in, a_6 became significant even when compared to the δ^* = ± 75 μm experiment, varying between 60 and 70 % (Fig. 8c and d). Again, the magnitude of a_5

remained constant after transition (Fig. 8d), and changes in total magnitude are a function α_6 activity corresponding to friction at the contact being exceeded.

(a)

(b)

(c)

(d)

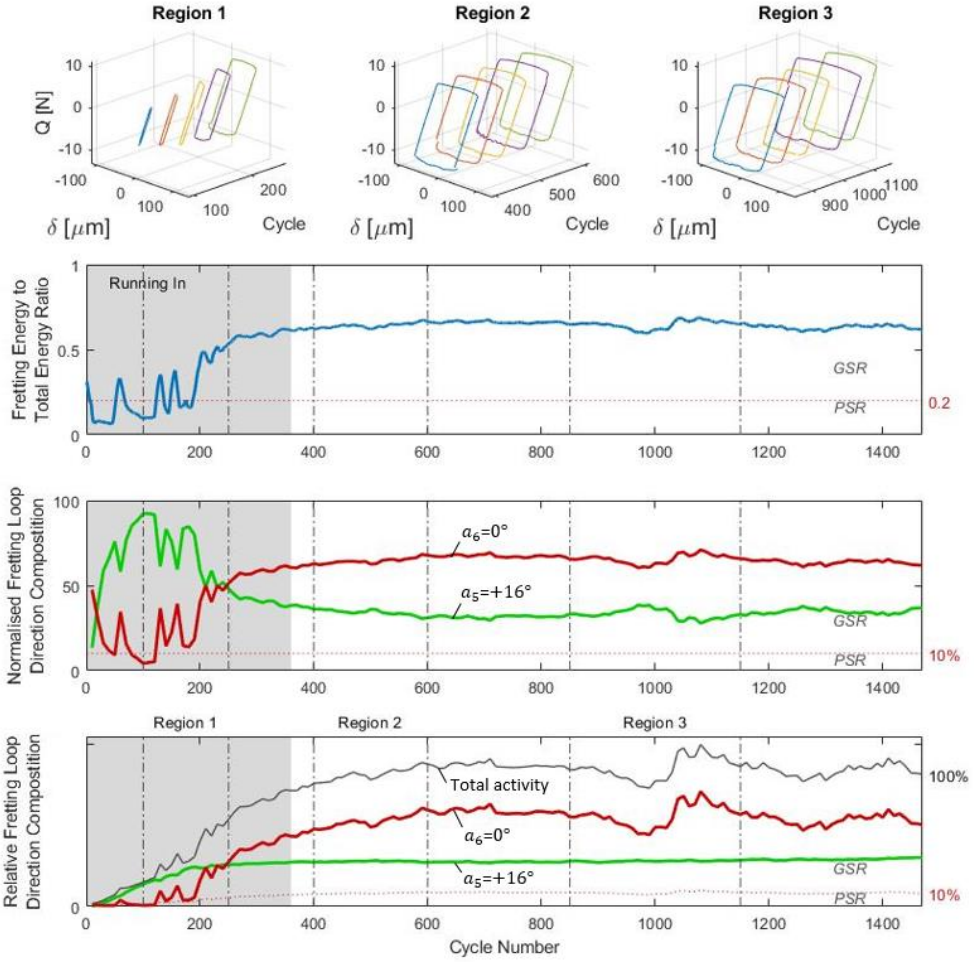

Fig. 8 The δ^* = ±100 μm experiment, *(a) fretting loops from three regions demonstrating representative fretting behaviour throughout the experiment: (i) Region 1 over transition according to the* 10 % α_6 *and 0.2 energy ratio thresholds (ii) Region 2 mid test and (iii) Region 3 towards the end of the test, (b) fretting energy to total energy ratio with the 0.2 threshold indicated, (b) fretting energy to total energy ratio with the 0.2 threshold indicated and, (c) normalised percentage fretting loop direction composition with 10 % threshold, (d)* the relative fretting loop direction composition with indicated 'Total activity' indicating 100 % total fretting loop vector magnitude (i.e. the total perimeter of the fretting loop) and threshold at 10% of the total activity. *The running in period is indicated at this shaded grey region in b, c and d.*

The percentage composition of α_6 and the 10 % threshold were used to identify transition points. *Fig. 9* demonstrates the transition point as each experiment progressed and the point at which the running-in period finished for easy identification between the PSR, MFR and GSR.

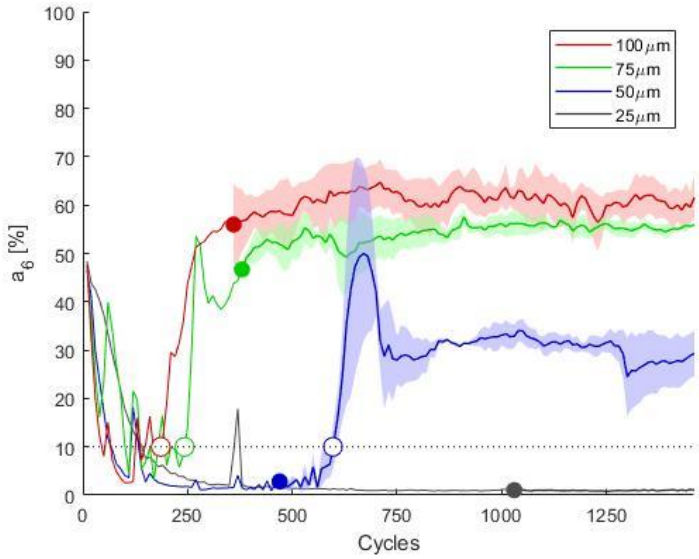

Fig. 9 Mean percentage a_6 composition where the shaded areas represent the standard deviation between the three repeats after the running in period, indicated as after the solid markers. The transition points from PSR to GSR are indicated by white circular markers outlined in the corresponding colour.

4. Discussion:

This study saw the development of a flexible loop analysis method that was able to quantify and characterise its constituent parts. This paper details its applicability to a fretting contact for transition identification independent of the contact geometry, contact compliance and working conditions. Transition identification was achieved using a 10 % threshold of a_6 (or '$a_{\left(\frac{N+1}{2}\right)}$' where N is an odd number) from the understanding that the presence of any pure slip indicates the GSR, underpinned by the regimes fundamental differences while allowing for experimental variation [7]. Interestingly this correlated very closely to the thresholds determined theoretically to overcome friction underpinned by Mindlin's work unlike transition identified using slip index [10,18,25]. This loop analysis offers additional insight into the stability of each regime as well as the onset of transition. Providing complementary information to other regime transition identification methods. Specifically, by understanding how stable each regime is, looking at the proportional composition and how compliant the contact is from assessment of the characteristic categories providing more information then fretting energy ratio, slip ratio and slip index used by literature [18,20,21,25,26].

The selected tangential displacements provided the PSR, MFR and GSR. Ito et al. used similar working conditions with the exception of a 130 MPa greater average contact pressure. They found that at $\delta^* = \pm 40\ \mu m$ and below the PSR was achieved and at $\delta^* = \pm 200\ \mu m$ the GSR was achieved [17]. Experimental working conditions applied in this work produced the three respective regimes summarised by the commonly used Running Condition Fretting Map (*Fig. 10*a) [8,27,28]. From results presented in *Fig. 9*, the dynamic transition between PSR and GSR as a function of applied displacement amplitude during the fretting test was easily identified. The "dynamic" context of the approach relates to the fact that the transition between the regimes can be pinpointed online during the test as a function of fretting cycles.

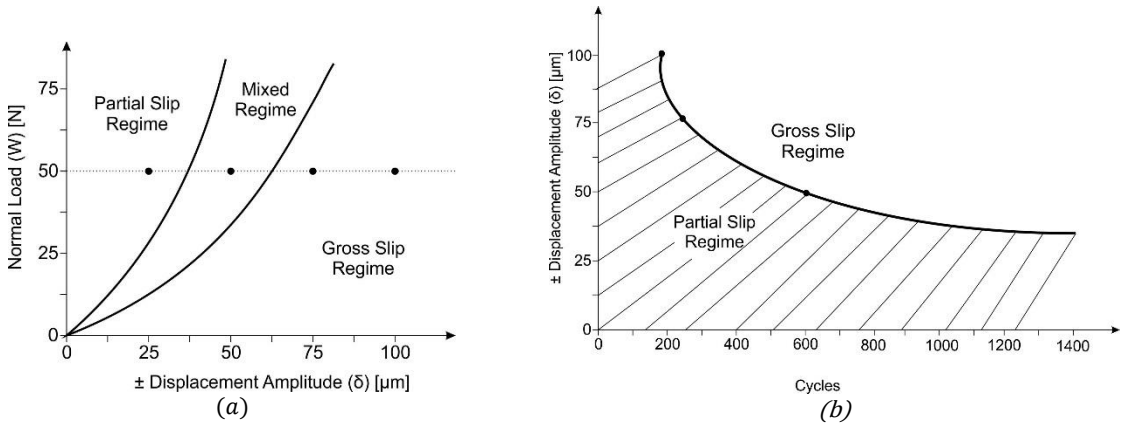

Fig. 10 (a) Running Condition Fretting Map. (b) Dynamic Fretting Transition Map indicating the fretting fatigue limit under steady state condition (i.e. excluding the running-in periods).

The gradient of the non-horizontal components of the fretting loops remains constant throughout the experiments, being a function of the materials response i.e. the elastic and plastic deformation of the contact (contact stiffness). This was demonstrated by only variations in a_5 and a_6 with absence of any significant activity in any other category. The plateau of a_5 as the fretting rig achieved steady state for all experiments (with the exemption of the $\delta^* = \pm 25\ \mu m$ experiment) indicated the point at which the contact stiffness was exceeded. The flexible nature of this method means that larger values of 'N' could theoretically identify the proportional composition of the elastic and plastic response of the contact however this was beyond the scope of this paper. Theoretically, if actual contact area (taking into account surface topography) and depth of material undergoing deformation could be measured, the shear modulus of the material could be calculated from the gradient of the elastic response of the contact.

Fretting energy ratio is used extensively to differentiate between regimes and closely agreed with regime transition identification using a 10 % a_6 composition threshold [20,21,26]. The 0.2 energy ratio threshold provided limited information on what was happening at the contact compared to the developed numerical method. The proportional composition of a_6 allowed determination of how stable the contact was within its respective regime, while the simultaneous proportional composition progression of the characteristic a_5 category provided information on how close the static friction of the contact is to being exceeded. This was demonstrated by fretting energy ratio for the $\delta^* = \pm 50\ \mu m$ and $\delta^* = \pm 75\ \mu m$ experiments suggesting the same regime. However, the simultaneous calculation of the proportional composition of a_6 and progression of the characteristic a_5 category provided easy identification of the MFR. This was achieved by identification of the steady state using the characteristic a_5 category.

The ability to characterise fretting loops and accurately identify transition points has many applications. For example it can be used for correlation testing between data sets for development of online asset monitoring devices, allowing adjustment of systems to prolong service and increase efficiency, supporting the concept of Industry 4.0 [29]. The additional information this method is capable of obtaining can also allow the prediction of the onset of transition with possible application as an early warning system. This loop analysis method could also aid the calculation of wear energy coefficients as an accurate slip amplitude is important in the development of tribologically critical engineering components and the development of coatings [12,30]. Previous studies have investigated fretting fatigue crack formation and fretting wear; the ability to know when to apply the correct

theory is possible with robust regime identfication and aided by a better understanding of the amount elastic and plastic compliance [2,30,31].

5. Conclusions

This study successfully developed a flexible loop analysis method based on simple vector principles, able to quantify and characterise its constituent parts. In summary this method:

- Provided a complementary method of regime transition identification to those based on theoretically overcoming friction at the contact.
- Quantify the proportion of pure slip and contact compliance, providing a better understanding of the stability of the regime.
- Proved to be repeatable under different test conditions and results were consistent to previous studies under similar working conditions.

This flexible loop analysis method has the potential to differentiate between elastic and plastic compliance of the contact however this was outside the scope of this paper. One potential limitation of this technique is that it is not easily applied for direct fretting regime transition detection in asset monitoring devices as tangential force and displacement are difficult to obtain outside of laboratory conditions. However, this technique offers an effective development tool for asset monitoring devices and tribologically critical engineering components and coatings. This is an extremely flexible technique that has applicability for other types of friction loop analysis.

6. Acknowledgments

Funding was provided by the EPSRC Centre for Doctoral Training for Integrated Tribology. Grant No. EPL01629X1

7. Declaration of Interest Statement

There were no conflicts of interest.

8. References

1. Makino T, Kato T, Hirakawa K. Review of the fatigue damage tolerance of high-speed railway axles in Japan. *Eng Fract Mech*. 2011;78(5):810-825. doi:10.1016/j.engfracmech.2009.12.013

2. Szolwinski MP, Farris TN. Mechanics of fretting fatigue crack formation. *Wear*. 1996;198(1-2):93-107. doi:10.1016/0043-1648(96)06937-2

3. Forsyth PJ. Fretting fatigue. In: Waterhouse RB (Robert B, ed. *Fretting Fatigue*. Applied Science; 1981:99.

4. Waterhouse RB. Fretting Corrosion. *Proc Inst Mech Eng*. 1955:1157-1172. doi:10.1016/B978-0-408-00109-0.50068-7

5. Brown SA, Flemming CAC, Kawalec JS, et al. Fretting corrosion accelerates crevice corrosion of modular hip tapers. *J Appl Biomater*. 1995. doi:10.1002/jab.770060104

6. Goldberg, J., Gilbert, J., Jacobs, J., Bauer, T., Paprosky, W. and Leurgans S. A Multicenter Retrieval Study of the Taper Interfaces of Modular Hip Prostheses. *Clin Orthop Relat Res*. 2002;401:149-161.

7. Vingsbo O, Söderberg S. On fretting maps. *Wear*. 1988;126(2):131-147. doi:10.1016/0043-1648(88)90134-2

8. Zhou ZR, Nakazawa K, Zhu MH, Maruyama N, Kapsa P, Vincent L. Progress in fretting maps. *Tribol Int*. 2006;39(10):1068-1073. doi:10.1016/j.triboint.2006.02.001

9. Zhou ZR, Fayeulle S, Vincent L. Cracking behaviour fretting wear of various aluminium alloys during. *Wear*. 1992;155:317-330. doi:10.1016/0043-1648(92)90091-L

10. Mindlin RD, Deresiewicz H. Elastic spheres in contact under varying oblique forces. *ASME Tram J Appl Mech*. 1953;20:327-344.

11. Zhou ZR, Vincent L. Mixed fretting regime. *Wear*. 1995;181-183(PART 2):531-536. doi:10.1016/0043-1648(95)90168-X

12. Liskiewicz T, Fouvry S. Development of a friction energy capacity approach to predict the surface coating endurance under complex oscillating sliding conditions. *Tribol Int*. 2005;38(1):69-79. doi:10.1016/j.triboint.2004.06.002

13. Varenberg M, Halperin G, Etsion I. Different aspects of the role of wear debris in fretting wear. *Wear*. 2002;252(11-12):902-910. doi:10.1016/S0043-1648(02)00044-3

14. Bill RC. The Role of Oxidation in the Fretting Wear Process. 1980.

15. Sauger E, Fouvry S, Ponsonnet L, Kapsa P, Martin JM, Vincent L. Tribologically transformed structure in fretting. *Wear*. 2000;245(1-2):39-52. doi:10.1016/S0043-1648(00)00464-6

16. Cadario A, Alfredsson B. Fretting fatigue experiments and analyses with a spherical contact in combination with constant bulk stress. *Tribol Int*. 2006;39(10):1248-1254. doi:10.1016/j.triboint.2006.02.012

17. Ito S, Shima M, Jibiki T, Akita H. The relationship between AE and dissipation energy for fretting wear. *Tribol Int*. 2009;42(2):236-242. doi:10.1016/j.triboint.2008.06.010

18. Fouvry S, Kapsa P, Vincent L. Analysis of sliding behaviour for fretting loadings: determination of transition criteria. *Wear*. 1995;185(1-2):35-46. doi:10.1016/0043-1648(94)06582-9

19. Fouvry S, Kapsa P, Vincent L. Developments of fretting sliding criteria to quantify the local friction coefficient evolution under partial slip condition. In: Elsevier; 1998:161-172. doi:10.1016/S0167-8922(98)80071-0

20. Fouvry S, Kapsa P, Zahouani H, Vincent L. Wear analysis in fretting of hard coatings through a dissipated energy concept. *Wear*. 1997;203-204(96):393-403. doi:10.1016/S0043-1648(96)07436-4

21. Fouvry S, Kapsa P, Vincent L. Description of fretting damage by contact mechanics. doi:10.1002/zamm.20000801311

22. Bryant M, Neville A. Fretting corrosion of CoCr alloy: Effect of load and displacement on the degradation mechanisms. *Proc Inst Mech Eng Part H J Eng Med*. 2017. doi:10.1177/0954411916680237

23. Heredia S, Fouvry S. Introduction of a new sliding regime criterion to quantify partial, mixed and gross slip fretting regimes: Correlation with wear and cracking processes. *Wear*. 2010;269(7-8):515-524. doi:10.1016/j.wear.2010.05.002

24. Suciu CV, Uchida T. Modeling and simulation of the fretting hysteresis loop. In: *Proceedings - International Conference on P2P, Parallel, Grid, Cloud and Internet Computing, 3PGCIC 2010*. ; 2010. doi:10.1109/3PGCIC.2010.96

25. Varenberg M, Etsion I, Halperin G. Slip index: A new unified approach to fretting. *Tribol Lett*. 2004;17(3):569-573. doi:10.1023/B:TRIL.0000044506.98760.f9

26. Fouvry S, Kubiak K. Introduction of a fretting-fatigue mapping concept: Development of a dual crack nucleation - crack propagation approach to formalize fretting-fatigue damage. *Int J Fatigue*. 2009;31(2):250-262. doi:10.1016/j.ijfatigue.2008.09.002

27. Zhang D, Shen Y, Xu L, Ge S. Fretting wear behaviors of steel wires in coal mine under different corrosive mediums. *Wear*. 2011;271(5-6):866-874. doi:10.1016/j.wear.2011.03.028

28. Xu J, Zhou ZR, Zhang CH, Zhu MH, Luo JB. An investigation of fretting wear behaviors of bonded solid lubricant coatings. *J Mater Process Technol*. 2007;182(1-3):146-151. doi:10.1016/j.jmatprotec.2006.07.023

29. Shrouf F, Ordieres J, Miragliotta G. Smart Factories in Industry 4 . 0 : A Review of the Concept and of Energy Management Approached in Production Based on the Internet of Things Paradigm. *Ieee Ieem*. 2014:697-701.

30. Fouvry S, Liskiewicz T, Kapsa P, Hannel S, Sauger E. An energy description of wear mechanisms and its applications to oscillating sliding contacts. *Wear*. 2003;255(1-6):287-298. doi:10.1016/S0043-1648(03)00117-0

31. Fouvry S, Kapsa P, Vincent L, Dang Van K. Theoretical analysis of fatigue cracking under dry friction for fretting loading conditions. *Wear*. 1996;195(1-2):21-34. doi:10.1016/0043-1648(95)06741-8